Ultrasound propagation through dilute polydisperse microbubble suspensions

Nicholas C. Ovenden[a)] & Jean-Pierre O'Brien
Department of Mathematics, University College London
Gower Street, London WC1E 6BT, United Kingdom

Eleanor Stride
Institute of Biomedical Engineering, Old Road Campus Research Building
University of Oxford, Oxford OX3 7DQ, United Kingdom

[a)]Corresponding Author. Email: n.ovenden@ucl.ac.uk

Abstract

In a fully nonlinear model of wave propagation through bubbly media, computational complexity arises when the medium contains a polydisperse bubble population. This is because a nonlinear ordinary differential equation governing the bubble response must be solved for the current radius of each bubble size present at every spatial location, and at every time step. In biomedical ultrasound imaging, commercial contrast agents typically possess a wide range of bubble sizes that exhibit a variety of differing behaviours at ultrasound frequencies of clinical interest. Despite the advent of supercomputing resources, the simulation of ultrasound propagation through microbubble populations still represents a formidable numerical task. Consequently, efficient computational algorithms that have the potential to be implemented in real time on clinical scanners remain highly desirable. In this work, we investigate a numerical approach that computes only a single ordinary differential equation at each spatial location which can potentially reduce significantly the computational effort. We demonstrate that, under certain parameter regimes, the approach replicates the fully nonlinear model of an incident ultrasound pulse propagating through a polydisperse population of bubbles with a high degree of accuracy.

Keywords: bubble dynamics; nonlinear wave propagation; contrast agents; layered media.

I Introduction

Gas microbubbles stabilised by a surfactant or polymer coating have now been in clinical use as contrast agents for ultrasound imaging for several decades[1]. They are widely used in echocardiography and, increasingly, for quantitative studies of tissue perfusion[2]. Despite their undoubted potential in these applications, obtaining reliable quantitative information still represents a considerable challenge in contrast imaging. It is the combination of a large effective scattering cross-section due to their compressibility and the non-linear response to ultrasound excitation that makes microbubbles such effective contrast agents. These properties, however, lead to significantly nonlinear propagation through regions of tissue containing microbubbles and both to image artefacts and difficulties in obtaining accurate quantitative information[3].

Several innovative strategies have been proposed in recent years to remove artefacts under certain situations[4]. The majority of quantitative imaging algorithms, however, rely on empirically derived correction factors and assume that both backscatter and attenuation increase linearly with microbubble concentration[3]. There are similarly very few theoretical models describing the response of a contrast agent population that take into account non-linear propagation and multiple bubble interactions. This is despite the fact[5] that a typical contrast agent suspension contains approximately 10^9 bubbles/ml giving rise to *in vivo* concentrations between 10^4 to 10^6 bubbles/ml (10^{10} to 10^{12} m^{-3}) depending on the dilution of the bolus (assuming an average human blood pool volume of 5 litres[6]).

Outside the contrast agent field, sound propagation through bubbly liquids has received considerably more attention. Theories of wave scattering in bubbly liquids have their origins in Lord Rayleigh's work in the 19th Century on light scattering[7]. Scattering of acoustic waves can also be traced back to work by Rayleigh[8] and Sewell[9] who investigated the propagation of sound through fog. These early theories focused on obtaining analytical solutions

to the relevant wave equations, whereas more recent research has been driven to a larger extent by tractable numerical computation. Classical scattering models require certain, quite severe, simplifying assumptions to be made in order to derive a closed-form solution. Aside from the fact that the scatterers must occupy a small volume fraction, the scatterers are typically assumed to behave linearly[10], a situation that is rarely the case with the use of bubbles in medicine. Previous work has examined weakly-nonlinear approximations to wave propagation in polydisperse bubble suspensions, building on earlier studies[11,12], which reduce the governing equations to either the nonlinear Schrödinger equation or Landau-Ginzburg equation[13]. It has also been shown under certain conditions that the propagation of finite amplitude long waves through polydisperse bubble suspensions can be approximated by a propagation model for a monodisperse gas population with effective physical parameters[14]. Some numerical simulations of shock propagation in polydisperse bubble suspensions have used an alternative approach of ensemble-averaged techniques to derive statistically-averaged conservation laws[15].

Van Wijngaarden[16] was the first author to present a model that took into account fully nonlinear bubble oscillations by matching the pressure and momentum changes between the liquid and the bubble. His results were subsequently rigorously proved by Caflisch et al.[17] and a numerical scheme for solving the model, in the form derived by Commander and Prosperetti[18], has been applied to microbubble contrast agent suspensions by various authors[19–21]. The model is valid for small gas-bubble volume fractions, neglects bubble interactions such as collisions, and assumes that the bubbles remain spherical at all times. The numerical scheme involves solving an inhomogeneous wave equation for the pressure $p(\boldsymbol{x}, t)$ (varying in space $\boldsymbol{x}$ and time t) travelling through a liquid with wavespeed c_0 and density ρ_0, where the forcing term models the average response of an effective medium composed of a population of $n(R_0)$ bubbles with initial and current radii R_0 and $R =$

$R(t; R_0, \boldsymbol{x})$ respectively,

$$\frac{1}{c_0^2}\frac{\partial^2 p}{\partial t^2} - \nabla^2 p = 4\pi\rho_0 \int_0^\infty \left[R^2 \frac{\partial^2 R}{\partial t^2} + 2R\left(\frac{\partial R}{\partial t}\right)^2 \right] n\big(R_0\big)\mathrm{d}R_0. \tag{1}$$

This equation can be discretised in space j and time s, by space- and time-steps of length Δx and Δt respectively, for each bubble of size R_k out of a total of N discrete bubble sizes in the population, using an explicit finite difference scheme that is accurate to second-order:

$$\begin{aligned} p_{j,s} &= 2p_{j,s-1} - p_{j,s-2} + c_0^2\Delta t^2 \left(\frac{p_{j+1,s-1} - 2p_{j,s-1} + p_{j-1,s-1}}{\Delta x^2} \right) \\ &+ 4\pi\rho_0 c_0^2 \Delta t^2 \sum_{k=1}^{N} n(R_k) \left[R_k^2 \, \ddot{R}_k + 2R_k \, \dot{R}_k^{\,2} \right]_{j,s-1}, \end{aligned} \tag{2}$$

where $\dot{R}_k\ (t)$ and $\ddot{R}_k\ (t)$ are the local kth bubble size's radial velocity and acceleration respectively.

Computational complexity arises when modelling a polydisperse bubble population. In equation (2), the bubble response for each equilibrium bubble size R_k must be computed to form the sum. For large values of N this becomes highly computationally intensive and hence cannot be easily implemented in real time for the purposes of analyzing clinical ultrasound data. An approach that significantly reduces the computational effort has been proposed by Hibbs et al.[22] whereby only one bubble size R_k is calculated at each spatial location in the mesh. The size of this bubble is chosen randomly according to a probability distribution defined by the discrete size distribution $n(R_k)$ and fixed at the start of the simulation. In this way it is possible to reduce the complexity of the problem at each point in space and time by a factor of N, and thus equation (2) is simplified to

$$p_{j,s} = 2p_{j,s-1} - p_{j,s-2} + c_0^2\Delta t^2 \left(\frac{p_{j+1,s-1} - 2p_{j,s-1} + p_{j-1,s-1}}{\Delta x^2} + 4\pi\rho_0 n_{\mathrm{tot}} \left[R_k^2 \ddot{R}_k + 2R_k \, \dot{R}_k^{\,2} \right]_{j,s-1} \right), \tag{3}$$

where $n_{\rm tot} = \sum_{k=1}^{N} n(R_k)$ is the total concentration of bubbles. The aim of this study is to investigate the accuracy and range of validity of this approximation, which shall be defined in this paper as the "homogeneous layer" (HL) approximation. If it can be shown that this yields valid results in certain parameter regimes then it could greatly simplify the computational complexity, leading to improvements in modelling and eventually, quantitative imaging applications.

II Equation of motion for microbubble dynamics

In order to solve any of the equations (1) - (3) a further equation describing the radial oscillations of a microbubble is required. There are several models describing the response of coated microbubbles to ultrasound excitation available in the literature, similar in form to the equation derived by Rayleigh, Plesset, Noltingk, Neppiras and Poritsky[23,24]. For the purposes of this study the following form[25,26] is adopted:

$$R_k(t)\ddot{R}_k(t)+\frac{3}{2}\,\dot{R}_k^{\,2}\,(t) = \frac{1}{\rho_0}\left(P_b\left(\frac{R_{0k}}{R_k}\right)^{3\gamma}+p_v-\frac{2\sigma(\Gamma)}{R_k}-\frac{4\mu_0\,\dot{R}_k}{R_k}-\frac{4\kappa_s\,\dot{R}_k}{R_k^2}-p_0-p(\boldsymbol{x},t)\right), \quad (4)$$

where the microbubble coating is represented by a surface tension, $\sigma(\Gamma)$, which depends on the surface concentration of surfactant Γ, as well as a shell viscosity, κ_s. The density and viscosity of the surrounding liquid are ρ_0 and μ_0 respectively. The ambient and vapour pressures are p_0 and p_v, and γ is the polytropic exponent defining the dynamic behaviour of the gas inside the bubble.

III Linear Theory

A Preliminaries

To compare the HL approximation in (3) to the fully polydisperse model, it is helpful to initially consider an analytical solution to the coupled equations (3) and (4) by assuming a time-harmonic incident wave of angular frequency ω. Equation (3) can be considered to be equivalent to approximating the effective medium as a series of "layers" of monodisperse bubbles. As a result, the HL approximation resembles propagation of a wave through layered media[27,28] where much work has been done in both quantum mechanics, optics and geophysics. More specifically, periodic-layered media has been studied extensively and this framework is adopted initially to analyse the HL approximation proposed above.

The simplest illustrative model of the HL approximation is to consider a bidisperse distribution of bubbles which is modelled as a periodic series of layers of equal width d, with each layer containing a single bubble size. The bubbles are assumed to exhibit small oscillations about their equilibrium size so that a linear approximation of (4) can be taken. The surface tension is also assumed to remain constant during the oscillations, so that $\sigma(\Gamma) = \sigma_0$. Let us suppose that the medium consists of $N+1$ layers of one bubble type (labelled 1) interspersed with layers of the second bubble type (labelled 2). The pressure pulse in the nth layer of bubbles of type 1 can be expressed in the following manner:

$$P_n(x,t) = \left\{ \hat{T}_n \, \mathrm{e}^{+\mathrm{i}k_1(x-(n+1)2d)} + \hat{R}_n \, \mathrm{e}^{-\mathrm{i}k_1(x-(n+1)2d)} \right\} \mathrm{e}^{-\mathrm{i}\omega t}, \tag{5}$$

which is valid in the region $2nd + d/2 < x < (2(n+1)d - d/2)$. The wavenumber k_j in each layer ($j = 1, 2$) is dependent on the equilibrium bubble size R_j of that individual layer, via the relation[10,18]

$$k_j^2 = \frac{\omega^2}{c_0^2} + 4\pi\omega^2 \frac{n_{\mathrm{tot}} R_j}{\omega_j^2 - \omega^2 - 2\mathrm{i}\delta_j\omega}. \tag{6}$$

Here, ω_j is the bubble's natural frequency and δ_j is the damping coefficient when approximating the bubble as a linear oscillator. Note that the difference in sign chosen for the $\mathrm{e}^{\pm \mathrm{i}\omega t}$ term here compared to Commander & Prosperetti[18] is taken into account.

By matching the pressure and axial velocity at each layer interface, an expression for the transmission coefficient can be derived in terms of the complex Bloch phase, γ, as follows[27,29]:

$$\frac{\hat{T}_N}{\hat{T}_0} = \frac{\sin\gamma}{\sin(N\gamma)P_{11} - \sin((N-1)\gamma)}, \tag{7}$$

where

$$\cos(\gamma) = \frac{1}{2}\mathrm{Tr}(\mathbf{P}) = \cos(k_1 d)\cos(k_2 d) - \frac{1}{2}\left(\frac{Z_1}{Z_2} + \frac{Z_2}{Z_1}\right)\sin(k_2 d)\sin(k_1 d), \tag{8}$$

and $Z_i = \rho_0\omega/k_i$ is the layer impedance. The form of expression (7) alludes to the emergence of permitted bands of the frequency spectrum that are transmitted almost perfectly as the number of layers increases, separated by gaps over which transmission is almost non-existent. However, in the case of bubble layers, γ is not real as the wavenumbers k_j are complex. The key parameter guiding the transmissive properties of the layered medium is the ratio of wavelength λ to layer thickness d, with very large λ/d leading to an "effective medium approximation" (high frequency approx) and λ/d small leading to a different "time-averaged" low-frequency approximation. Hovem[30] used an eigenvalue analysis to determine the critical λ/d separating these two regimes and Stovas and Arntsen[31] showed that a transition region occurs between the two regimes, the extent of which depends on the difference in layer impedances.

While our bubble-layer model is not completely analogous to the models of layered media in seismic or quantum theory, it remains important to heed the observations above. For sufficiently low pressure amplitudes and/or bubble concentrations a population of polydisperse bubbles is expected to behave as an effective medium[18], with the wavenumber k_{eff}

given by

$$k_{\text{eff}}^2 = \frac{\omega^2}{c_0^2} + 4\pi\omega^2 \int_0^\infty \frac{R_0 n(R_0)}{\omega_N^2(R_0) - \omega^2 - 2\mathrm{i}\delta(R_0)\omega} \mathrm{d}R_0. \tag{9}$$

For our bidisperse case, this means that $k_{\text{eff}}^2 = \left(k_1^2 + k_2^2\right)/2$. The HL approach in the linear regime should therefore be expected to approximate well the transmission coefficient of the effective medium, given by

$$\left| \frac{\hat{T}_N}{\hat{T}_0} \right| \approx \left| \mathrm{e}^{+\mathrm{i}k_{\text{eff}}2dN} \right|. \tag{10}$$

Hibbs et al.[22] used ten points per wavelength in their finite-difference scheme for the HL approach. However, they did not vary the bubble type used at every grid point, which would yield $\lambda/d = 10$, but kept the same bubble size for several grid points in order that the layer thickness equalled the mean microbubble separation distance, $d = n_{tot}^{-1/3}$, where n_{tot} is the total bubble concentration. Table I shows the ratios λ/d thus obtained for typical microbubble concentrations and incident ultrasound frequencies. Note that the λ/d ratios

Table I: Values of λ/d based on layer width equalling the mean bubble separation distance

Frequency	0.5MHz	1.0MHz	1.75MHz	2.25MHz	3.5MHz
$n_{tot} = 5.5 \times 10^9 \mathrm{m}^{-3}$	5.3	2.6	1.5	1.2	0.8
$n_{tot} = 5.5 \times 10^{10} \mathrm{m}^{-3}$	11.4	5.7	3.3	2.5	1.6
$n_{tot} = 5.5 \times 10^{11} \mathrm{m}^{-3}$	24.6	12.2	7.0	5.5	3.5

used for the numerical results obtained by Hibbs et al.[22] (and, indeed, nearly all the ratios in the table) predominantly lie in the region referred to by Stovas and Artnsen[31] as the transition region, in which any layering of the medium could have a significant effect on the transmitted wave. This is undesirable as the layering is a modelling construction here and not a physical attribute of the real bubbly medium that is being simulated.

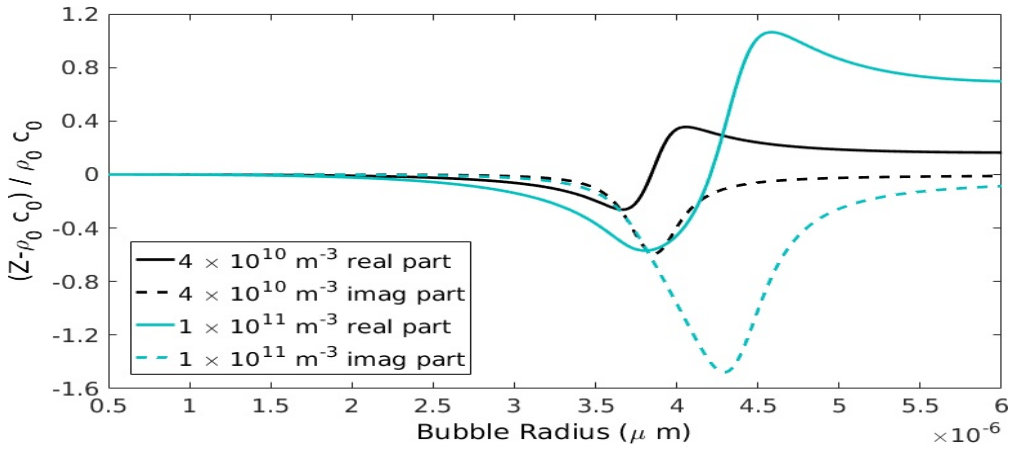

(a) Incident Frequency 1MHz

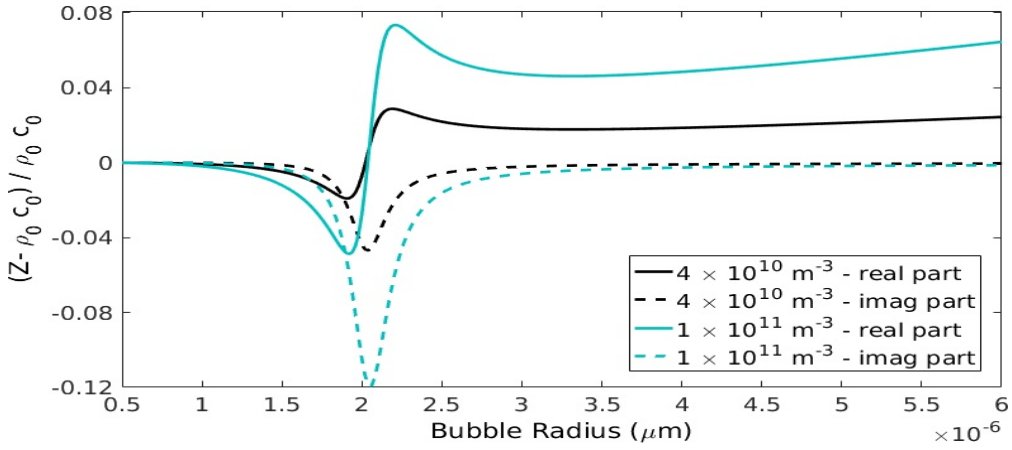

(b) Incident Frequency 2MHz

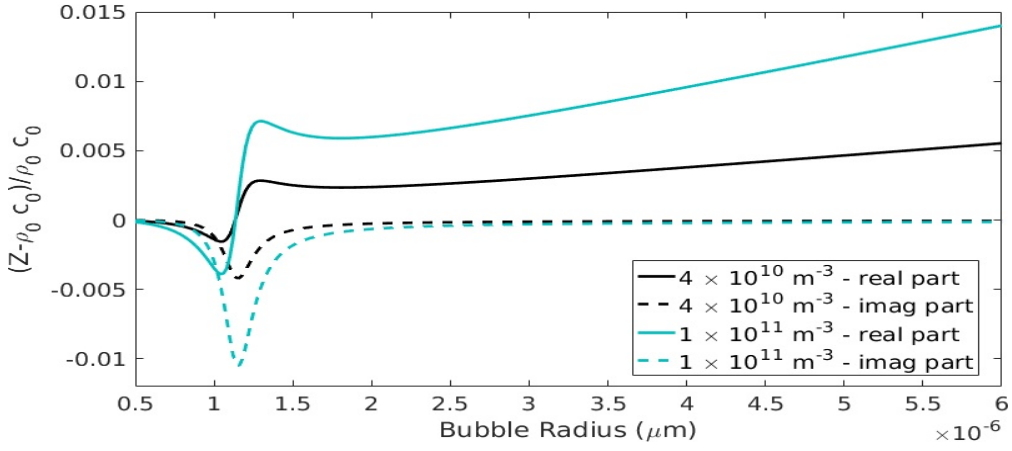

(c) Incident Frequency 4MHz

Figure 1: How the relative impedance of a homogeneous bubble layer varies with equilibrium bubble radius.

B Layered medium results

The periodic-layered theory is now applied to linear theory for ultrasound propagation through a microbubble cloud made up of bubbles of two distinct equilibrium radii, R_1 and R_2, which are present in equal amounts with an overall bubble concentration of n_{tot} per metre cubed. The impedance $Z_i = \rho_0\omega/k_i$ of a layer of monodisperse bubbles is the most crucial physical parameter here. The relative variation in layer impedance with equilbrium bubble radius, compared to the impedance of a medium with no bubbles, is shown in Fig. 1 for two different bubble concentrations ($n_{tot} = 4 \times 10^{10}$ and 1×10^{11} bubbles per m^3) and three different frequencies (1, 2 and 4 MHz). The values of the physical parameters used to determine the relevant layer impedances are as follows: $p_0 = 101.3\,\mathrm{kPa}$, $p_v = 2\,\mathrm{kPa}$, $\mu_0 = 10^{-3}\,\mathrm{kgm^{-1}s^{-1}}$, $\rho_0 = 10^3\,\mathrm{kgm^{-3}}$, $c_0 = 1500\,\mathrm{ms^{-1}}$, $\gamma = 1.4$, and $\sigma_0 = 0.07\,\mathrm{kgs^{-2}}$. The natural frequency and damping coefficient are calculated from the expressions

$$\omega_N^2(R_j) = \frac{(3\gamma(p_0 - p_v + 2\sigma_0/R_j) - 2\sigma_0/R_j)}{\rho_0 R_j^2}, \quad \delta(R_j) = \frac{4\mu_0}{\rho_0 R_j^2}.$$

The main features of Fig. 1 are that the layer impedance tends to vary greatly around the resonant bubble size (about 1.2μm radius at 4MHz, 2μm radius at 2MHz and 3.7μm radius at 1MHz), and the layer impedance remains markedly different from the ambient impedance for bubbles the natural frequency of which is lower than the driving frequency.

Our first example is a bidisperse population of bubble radii $R_1 = 1.8\mu$m and R_2, where R_2 lies in the range 1.9μm to 2.2μm at a bubble concentration of $n_{tot} = 10^{11}$ bubbles/m^3, with an incident frequency of 2MHz. The transmission coefficient of an incident wave over 5 incident wavelengths (3.7mm) is calculated for a period arrangement of layers of equal width d and this is compared to the transmission coefficient of an effective medium of an equal mixture of both bubble sizes. The relative error between the layered medium and the effective medium is given by $\left|\frac{\hat{T}_N}{\hat{T}_0}\right| \mathrm{e}^{+\mathrm{Im}(k_{\mathrm{eff}})2dN} - 1$, and this relative error is plotted against

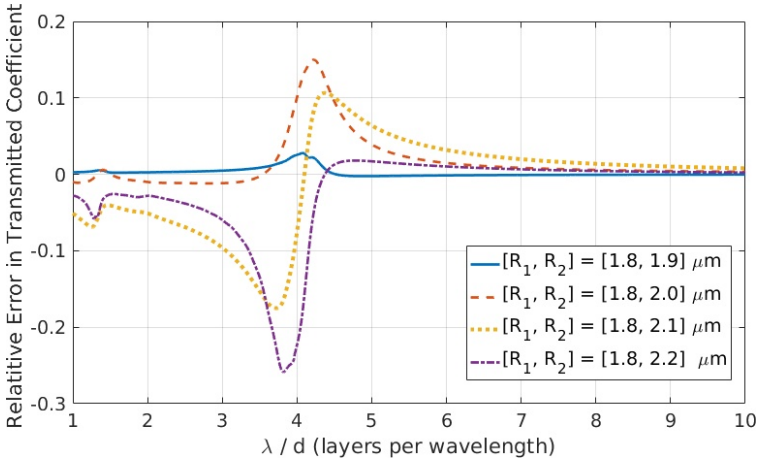

Figure 2: Incident Frequency 2MHz - variation in the transmission coefficient at a distance of five incident wavelengths obtained by propagation of a time-harmonic wave through a periodic arrangement of homogeneous bubble layers at a bubble concentration of $10^{11}\,\mathrm{m}^{-3}$.

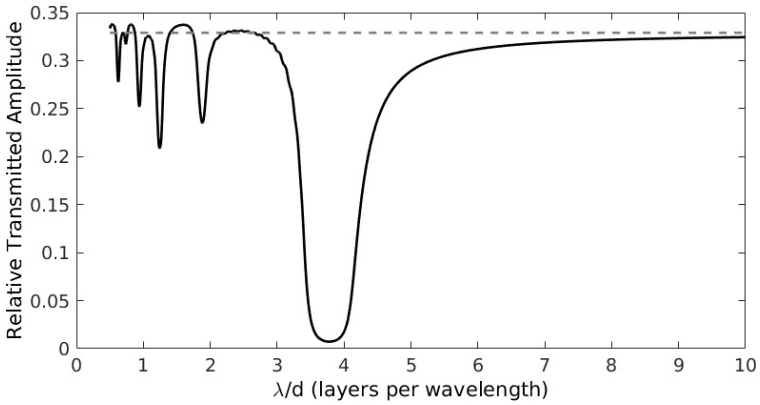

Figure 3: Incident Frequency 2MHz - variation in the transmission coefficient at a distance of 10 incident wavelengths obtained by propagation of a time-harmonic wave through a periodic layered arrangment of homogeneous bubble layers containing bubble sizes $R_1 = 1\mu$m and $R_2 = 4e-6\mu$m at a bubble concentration of $4 \times 10^{11}\,\mathrm{m}^{-3}$. The solid line is for the layered medium whereas the dashed line is the transmission amplitude for an effective medium.

the λ/d ratio in Fig. 2. Two important features can be observed here. First, there is good agreement between the HL and effective medium approaches for $\lambda/d \gtrsim 10$. Second, however, there are large relative errors in all the populations for $3 < \lambda/d < 5$ which corresponds to the transition region highlighted in seismological literature[31,32]. In line with the values in Table I, if d were made equal to the mean bubble separation distance in this case, then $\lambda/d = c_0(n_{tot})^{1/3}/f \approx 3.5$.

Resonant bubbles represent one important issue and, of course, a linear analysis cannot fully describe the relevant dynamics. Layers containing bubbles much larger than the resonant bubble size can also have a significant impact on transmission. Fig. 3 shows the transmitted coefficient (solid line) of a sinusoidal (time-harmonic) ultrasound wave of frequency 2MHz propagating ten incident wavelengths through a periodic layered medium containing layers of width d of bubbles of radius $R_2 = 4\mu$m, interspersed by bubble layers of width d containing bubbles of radius $R_1 = 1.6\mu$m at a concentration of 4×10^{11} bubbles per m^3. If the cell mimicked an effective medium then the transmitted amplitude would be the horizontal dashed line. Most notably, a band-like structure emerges in this situation with transmission loss occurring at certain λ/d ratios. A similar shielding phenomenon has been documented for the case of bubbles inside a sphere[33] but, to the best of the authors' knowledge, has not been mentioned elsewhere in the literature.

Our final result for periodic layered media is shown in Fig. 4 and is similar to that shown in Fig. 2 but for a lower frequency and lower concentration. In this scenario, one equilibrium bubble size has $R_2 = 3.5\mu$m (smaller than resonant size) with the other having radius R_1 in the range 1μm to 4.7μm. Due to the higher attenuation in this case, the comparison with the effective medium is made through propagation over the distance of a single wavelength. Note that, as in Fig. 2, λ/d ratios around 4 display very large deviations from the behaviour of an effective medium, but what is noteable in this case is that for $\lambda/d \approx 10$ differences of

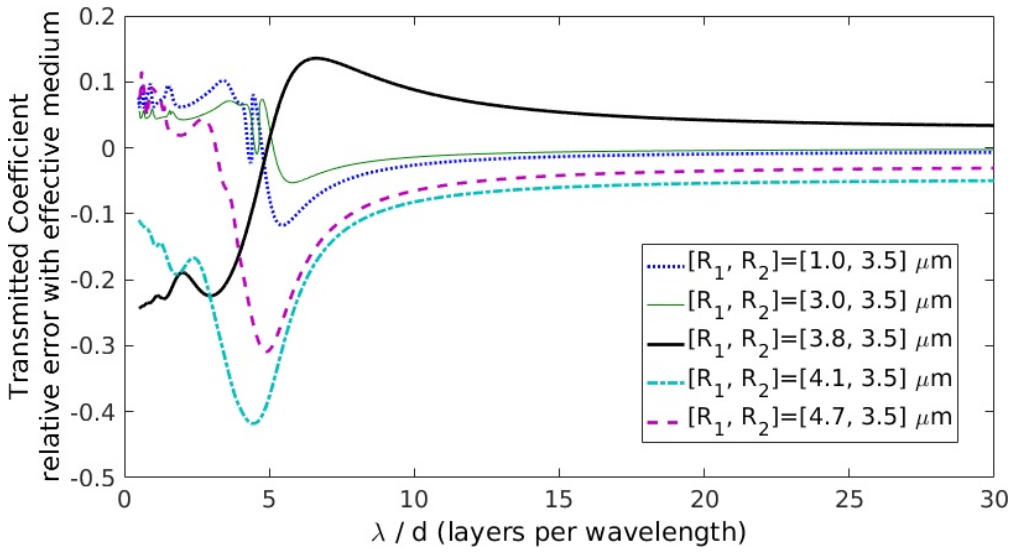

Figure 4: Incident Frequency 1MHz - variation in the transmission coefficient at a distance of a single incident wavelength obtained by propagation of a time-harmonic wave through a periodic arrangment of homogeneous bubble layers containing bubbles of radii R_1 and R_2 at a bubble concentration of $5.5 \times 10^{10}\,\mathrm{m}^{-3}$.

10% or more persist and, for even larger values of λ/d, there appears to be extremely slow, if any, convergence towards the effective medium behaviour (10) as $\lambda/d \to \infty$.

Of course, the proposed HL approximation is based on a random selection of layers as opposed to a periodic layering as above. Indeed if, for the bidisperse populations of bubbles discussed above, random selection were used then adjacent cells would frequently be of the same type. This, in turn, would reduce λ/d by a factor of 2 or more pushing the layered medium towards a lower average λ/d ratio, possibly leading to a larger divergence from effective medium behaviour. For a polydisperse bubble population, such as that of the commercial agent SonoVue®, it is expected that divergence from the effective medium prediction could occur due to reflections at each layer interface. However, whether these

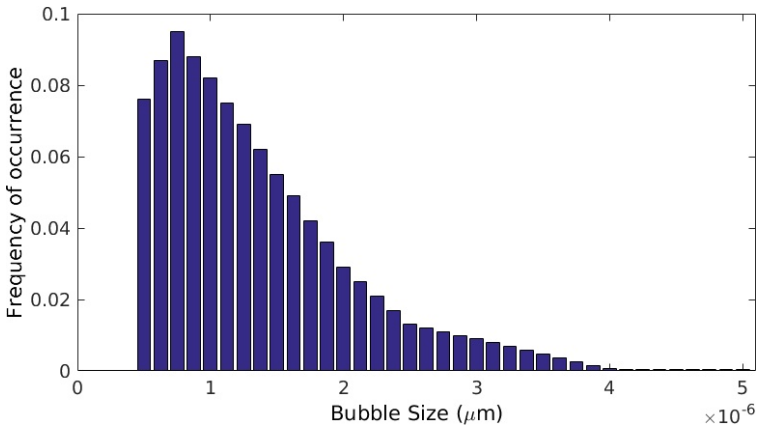

Figure 5: SonoVue®- distribution of equilibrium bubble sizes obtained by Gorce et al.[5].

errors would accumulate or cancel each other out is not clear. To test this idea, consider a layered medium of $(N+1)$ layers, with each layer having its own specific wavenumber k_n and impedance $Z_n = \rho_0\omega/k_n$ for $n = 1, \ldots, N+1$. The pressure field in the nth layer can be written in the form

$$P_n(x,t) = \left(T_n\,\mathrm{e}^{+\mathrm{i}k_n[x-(n-1)d]} + R_n\,\mathrm{e}^{-\mathrm{i}k_n[x-(n-1)d]}\right)\mathrm{e}^{-\mathrm{i}\omega t}\,. \tag{11}$$

As in the periodic case, the relationship between the transmission and reflection coefficients for adjacent layers is easily formulated and, from this, the transmission coefficient through $N+1$ such layers $|T_N|$ may be obtained via solving the expression

$$\begin{pmatrix} 1 \\ R_0 \end{pmatrix} = \mathbf{\Omega_1}\ldots\mathbf{\Omega_N}\begin{pmatrix} T_N \\ 0 \end{pmatrix}, \tag{12}$$

where

$$\mathbf{\Omega_n} = \begin{pmatrix} \frac{1}{2}\,\mathrm{e}^{-\mathrm{i}k_{n-1}d}\left(1+\frac{k_n}{k_{n-1}}\right) & \frac{1}{2}\,\mathrm{e}^{-\mathrm{i}k_{n-1}d}\left(1-\frac{k_n}{k_{n-1}}\right) \\ \frac{1}{2}\,\mathrm{e}^{+\mathrm{i}k_{n-1}d}\left(1-\frac{k_n}{k_{n-1}}\right) & \frac{1}{2}\,\mathrm{e}^{+\mathrm{i}k_{n-1}d}\left(1+\frac{k_n}{k_{n-1}}\right) \end{pmatrix}. \tag{13}$$

Utilising this approach, we adopt a set-up originally presented by Hibbs et al.[22] wherein a size distribution from Gorce et al.[5] for SonoVue® is used at a concentration of 5.5×10^{10}

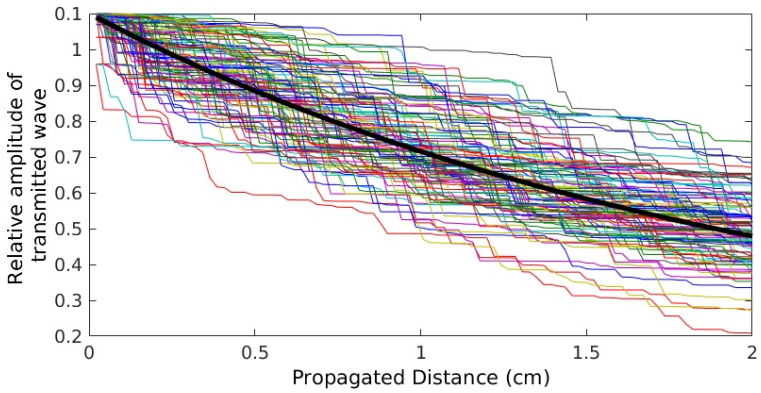

(a) Incident Frequency 1.75MHz, $\lambda/d = 4$ (based on Hibbs et al approach[22]) - 100 computations

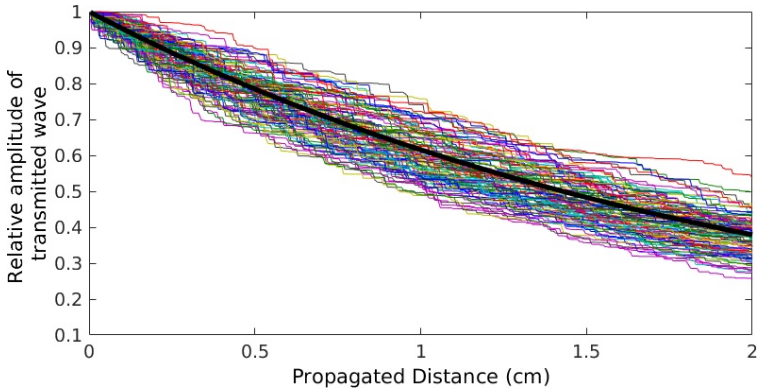

(b) Incident Frequency 1.75MHz, $\lambda/d = 20$ - 100 computations

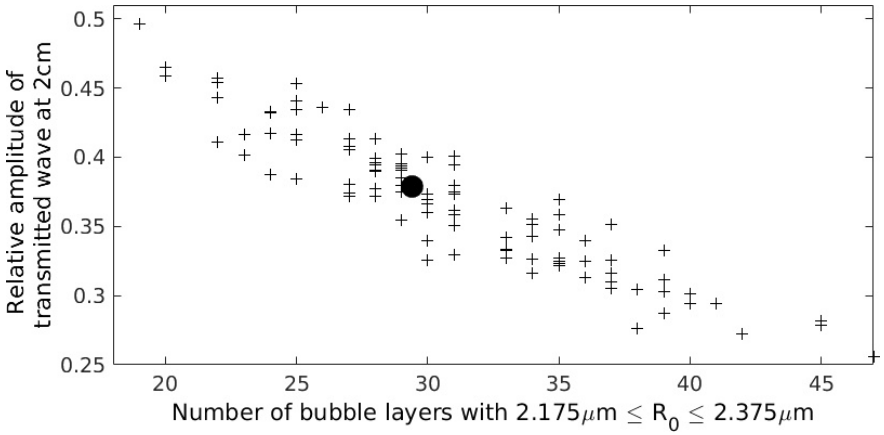

(c) Incident Frequency 1.75MHz, $\lambda/d = 20$, - 100 computations. Transmitted amplitude versus the number of resonant bubble layers. The solid circle represents the expected number of resonant bubble layers based on the bubble frequency distribution and the transmitted amplitude obtained by an effective medium.

Figure 6: Incident Frequency 1.75MHz Simulating propagation through SonoVue® (concentration $5.5 \times 10^{10}\mathrm{m}^{-3}$) using the HL approach and linear theory.

bubbles per m^3 and with a time-harmonic incident wave of frequency 1.75MHz. The λ/d ratio is fixed and the transmitted coefficient is computed through 1 up to N layers using equations (13) and (12), with the first and final layers being a quiescent medium with no bubbles so that $k_0 = k_N = \omega/c_0$. The maximum number of layers computed is determined by fixing the propagation distance at 2cm so that $Md = 0.02$m and the bubble type for each layer is chosen at random from the Gorce et al. distribution[5] depending on each bubble size's relative frequency (Fig. 5). Figs. 6a and 6b show the transmitted amplitude in the medium for one hundred independent computations with bubble types chosen at random for two different λ/d ratio cases. The transmitted amplitude for the effective medium with wavenumber k_{eff} is shown for comparison. In Fig. 6a, the chosen λ/d value is roughly based on the mean separation difference as in Hibbs et al[22]; this would mean $\lambda/d = 3.25$ which, for our simulation, is rounded up to four for convenience. A huge spread in the predicted attenuation at 2cm is apparent. What is somewhat surprising, however, is that while increasing the λ/d ratio to 20 in Fig. 6b leads to some reduction in the spread of transmission amplitudes obtained, it still remains significantly large with a greater than 20% difference in the transmitted amplitude at 2cm observed across 100 runs.

On closer inspection of the bubble types chosen for each layer there is a reasonably strong correlation between the number of resonant layers in the HL medium and the transmitted amplitude (Fig. 6c). One relatively straightforward way of therefore improving the HL approximation could be to take the expected number of layers of each bubble size from the distribution and allocate these layers in a random order; we describe this method of random selection as "selection without replacement" for the remainder of the paper. Fig. 6c, however, shows that, even across the runs containing the expected number of resonant bubble layers, a smaller but still significant variation in the predicted transmitted amplitude remains due to the layering alone.

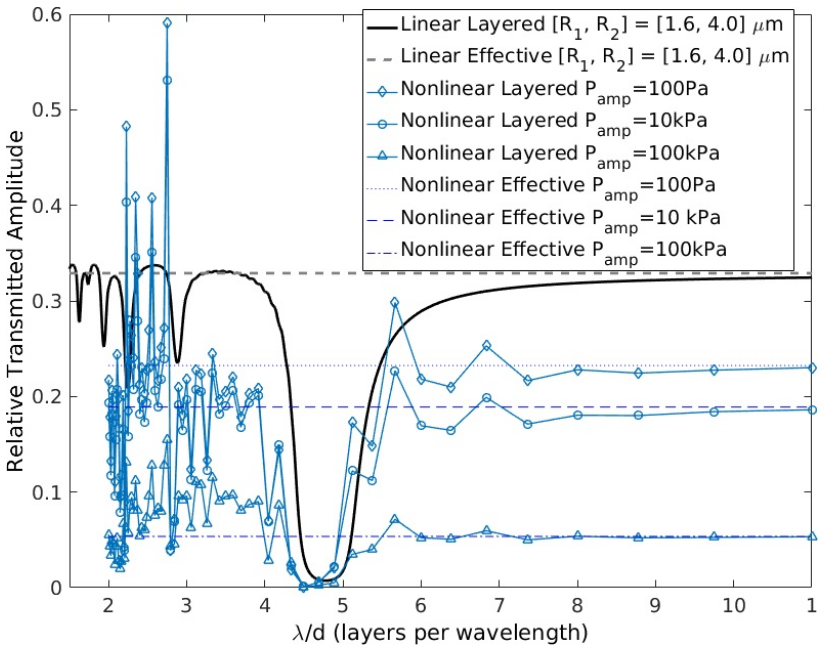

Figure 7: Incident frequency 2MHz - nonlinear propagation of an ultrasound pulse through periodic bubble layers at a concentration of $4 \times 10^{11} \mathrm{m}^{-3}$. Propagation distance is 10 incident wavelengths. Comparison of transmitted amplitudes to that obtained by linear theory and to that obtained by linear and nonlinear effective media.

IV Nonlinear simulations

The linear theory employed above provides some useful insight into the effect of wavelength-to-layer-width ratio and the possible occurrence of shielding phenomena in applying the HL approach as an approximation to ultrasound propagation through a polydisperse bubble cloud. Moreover, the linear theory suggests that the original HL approach proposed by Hibbs et al.[22] (henceforth referred to as **HLv1**) could potentially be improved as an approximation to the fully polydisperse model, without additional computational effort, by (i) randomly selecting the bubble layers *without replacement* so that the number of layers of each bubble

type/size equals the expected number (henceforth referred to as **HLv2**); and (ii) randomly selecting bubble layers without replacement, as in (i), but also selecting a different random bubble size at *every grid point* to maximize λ/d to equal the points per wavelength of the numerical calculation (henceforth referred to as **HLv3**). In the majority of medical applications, the population is sufficiently polydisperse and the pressure amplitude sufficiently high that there will always be some bubbles responding in a nonlinear manner. Therefore, we must now see if similar effects are observed in more clinically-relevant fully nonlinear cases that involve higher pressures amplitudes, resonant bubbles and varying surface tension. In this section, fully nonlinear computations are carried out using the wave equations (2) and (3) coupled to equation (4), for ultrasound propagation through a medium containing a polydisperse bubble population. Initially we simulate a bidisperse population of bubbles to see if shielding effects can be observed in the layered model for the nonlinear case. Following this, we examine the accuracy of the original HLv1 approach for the fully nonlinear computation with a polydisperse bubble cloud based on SonoVue® and then determine whether this accuracy can be improved by the proposed modified approaches, HLv2 and HLv3, and if an optimal way exists to reduced computational effort while preserving reasonable accuracy.

A Simulation parameters and numerical scheme

The parameter values used for the numerical simulations are as follows: $p_0 = 100\,\mathrm{kPa}$, $p_v = 0\,\mathrm{kPa}$, $\mu_0 = 10^{-3}\,\mathrm{kgm^{-1}s^{-1}}$, $\rho_0 = 10^3\,\mathrm{kgm^{-3}}$, $c_0 = 1500\,\mathrm{ms^{-1}}$, $\gamma = 1.4$, and $\kappa_s = 4 \times 10^{-9}\,\mathrm{kgs^{-1}}$. The simulations presented are restricted to non-destructive pressures where the incident pressure amplitude varies from 0.1kPa to 200kPa for a six-cycle Gaussian-enveloped incident pulse at frequencies 1, 2, 4 and 7.5 MHz. These simulated pulses propagate distances up to a few centimetres through the microbubble suspension, the concentration of which varies from 10^{10} bubbles/m^3 to 10^{12} bubbles/m^3. The individual bubbles are assumed to be

governed by the nonlinear equation (4) with varying surface tension. Shedding of surfactant such as discussed in previous work[21,34] is ignored in these computations so that the amount of surfactant on the bubble surface remains constant. The variation in coating parameters between different bubbles, which contributes to a spread of resonance frequencies in practice, is also neglected. Consequently, the surface tension can be expressed as a function of radius, given here by the previously adopted sigmoidal form[21]

$$\sigma(R) = \sigma_0 + \frac{\sigma_{\min} - \sigma_0}{\Big(1 + Q\exp\big(-U(R_0^2/R^2 - W)\big)\Big)^{(1/Y)}}, \tag{14}$$

where $\sigma_0 = 0.07\,\mathrm{kgs}^{-2}$, $\sigma_{\min} = 10^{-3}\,\mathrm{kgs}^{-2}$, $Q = 0.9799$, $U = 138.8$, $W = 0.9814$, and $Y = 2.926$. Two types of bubble population are investigated: a bidisperse population containing two different bubble sizes, to determine the possibility of shielding artefacts from the use of the HL approximation, and a polydisperse bubble population based on experimental measurements[5] of the commercial contrast agent SonoVue®.

For all numerical computations, equations (2) and (3) were nondimensionalised in time based on the centre frequency of the incident ultrasound pulse, f, and in space on the incident wavelength, *i.e.* c_0/f. Pressure was nondimensionalised on the amplitude of the incident pulse. The equations were solved using the explicit finite-difference scheme as written, and a fourth-order Runge Kutta method used for the bubble equation of motion (4), with bubble radius non-dimensionalised on a mean bubble radius (typically 2μm). The simulations presented throughout have $c_0\Delta t/\Delta x = 2/3$ (where Δt and Δx are dimensional) to satisfy the Courant condition and thus ensure stability of the explicit scheme. However, as the speed of sound in a bubbly medium can be much higher than that of the unbubbly medium, numerical tests were carried out on propagation through polydisperse microbubble suspensions using the following range of timestep ratios: $c_0\Delta t/\Delta x = 5/6,\ 2/3,\ 1/2$ and $1/3$. These tests confirmed that for SonoVue®, across all frequencies and concentrations of

interest, the numerical scheme was stable and accurate spectra obtained, with noticeable differences in spectra appearing only in the highly attenuated third and higher harmonics. The results from the numerical tests are in line with linear theory, where calculations of ω/k_{eff} using (9) indicate that the sound speed of the medium containing a SonoVue® bubble population is unlikely to exceed $1.05 \times c_0$ for all concentrations and frequencies examined.

B Bidisperse bubble populations

Populations containing equal proportions of two bubble sizes were numerically investigated in order to determine if shielding also occurs in the nonlinear regime. The first case considered is a fully nonlinear version of the shielding case seen in Fig. 3 with bubble sizes $[R_1, R_2] = [1.6, 4.0]\mu$m. Three six-cycle Gaussian envelope pulses of incident frequency 2MHz with maximum amplitudes 10Pa, 10kPa and 100kPa respectively propagate through ten incident wavelengths of alternate layers of each bubble size. The computational spatial step size was set at 70 points per wavelength and the number of discrete spatial points was varied from 1 to 70 leading to a range of λ/d from 1 to 70. Figure 7 shows the results of these computations for the three different amplitudes compared to the linear layered theory as well as to both linear and nonlinear effective media. The shielding behaviour predicted between $3.5 < \lambda/d < 4$ seems to be replicated almost identically (bar a slight shift) in the nonlinear cases and a similar shielding for $\lambda/d \approx 1.8$ is also replicated in the nonlinear case. We note that this agreement occurs in spite of the fact that the nonlinear incident wave is *not* time-harmonic and that the bubbles are now behaving fully nonlinearly with varying surface tension.

Moving on to our second presented case at a higher incident frequency, similar shielding phenomena and good agreement between linear theory and nonlinear computation still occur as shown in Fig. 8. In this case, a six-cycle Gaussian-enveloped pulse of incident frequency

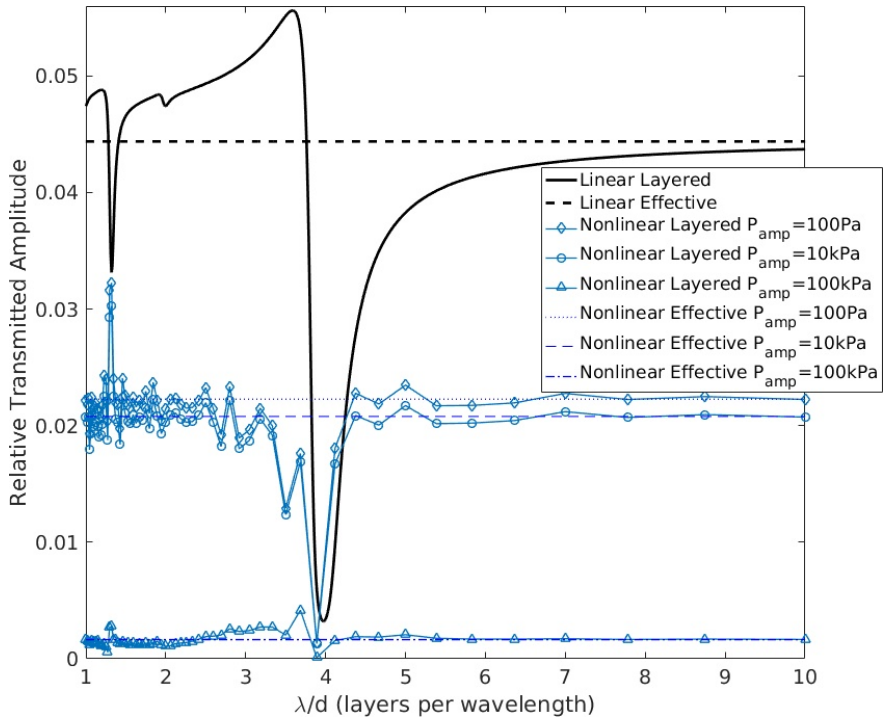

(a) 100Pa, 10kPa and 100kPa nonlinear ampltudes versus linear theory.

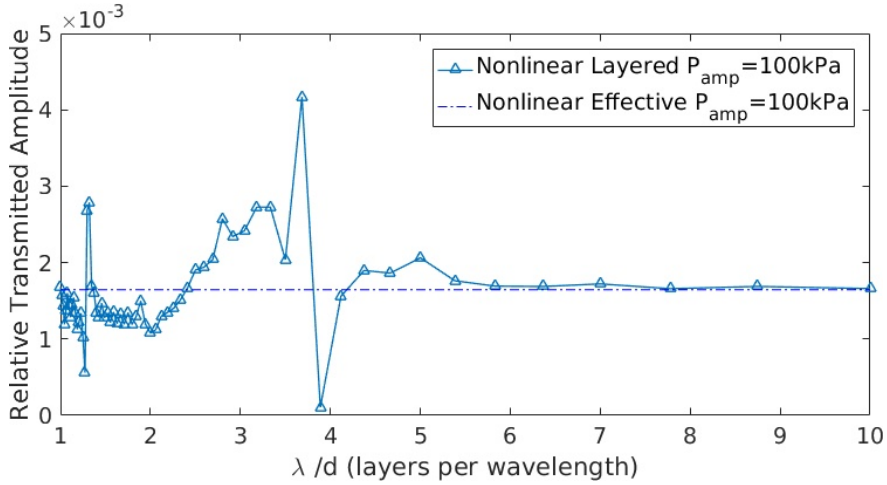

(b) 100kPa nonlinear amplitude case (zoomed in).

Figure 8: Incident frequency 4MHz - nonlinear propagation of an ultrasound pulse through a periodic bubble layers at a concentration of $1 \times 10^{12}\,\mathrm{m}^{-3}$. Propagation distance is 1 cm (27 incident wavelengths). Comparison of transmitted amplitudes to that obtained by linear theory and to that obtained by linear and nonlinear effective media.

4MHz propagates through layers of bubbles of alternate sizes 1 and 2μm. Fig. 8(a) shows the result from linear theory for a time-harmonic incident wave in addition to the nonlinear computations for maximum incident pulse amplitudes of 100Pa, 10kPa and 100kPa. Fig. 8(b) is then a zoomed-in view of the highest-amplitude 100kPa case, which still exhibits a similar transmitted amplitude response to that predicted by the linear theory, including a rise in transmitted amplitude around $\lambda/d \approx 3.6$, lying just to the left of the predicted drop in amplitude at $\lambda/d \approx 3.9$.

C Polydisperse bubble populations

Our presented simulations now turn to the more realistic and clinically relevant situation of a commercial contrast agent containing a polydisperse bubble population. As in Sec. III.B, we again adopt the size distribution of Gorce et al.[5] for SonoVue® that characterises the bubble size distribution into 37 distinct radii. A nonlinear propagation code was validated for different grid spacings and, as a result, a fully nonlinear polydisperse computation of equations (2) and (4), where all bubble sizes are computed at each grid point, using 70 points per wavelength was chosen as the "gold" standard benchmark to which all results obtained from the HL approximation are compared. In all cases, the incident wave is a six-cycle Gaussian-enveloped pulse, at ultrasound frequencies 1, 2, 4 and 7.5 MHz and with maximum amplitude ranging from 10Pa to 200kPa, that propagates a distance of 2cm through a SonoVue® population at concentrations of 10^{10}, 10^{11} and 10^{12} bubbles/m^3.. The surface tension of the bubbles is assumed to vary according to Eq. (14). For the HL approximation, computations using the original HL approach (HLv1) and the modified approaches, HLv2 and HLv3, are shown and analysed. We note here that in terms of the computing effort required for the HL approximation model, (3) and (4), HLv1, HLv2 and HLv3 all have the same computational cost.

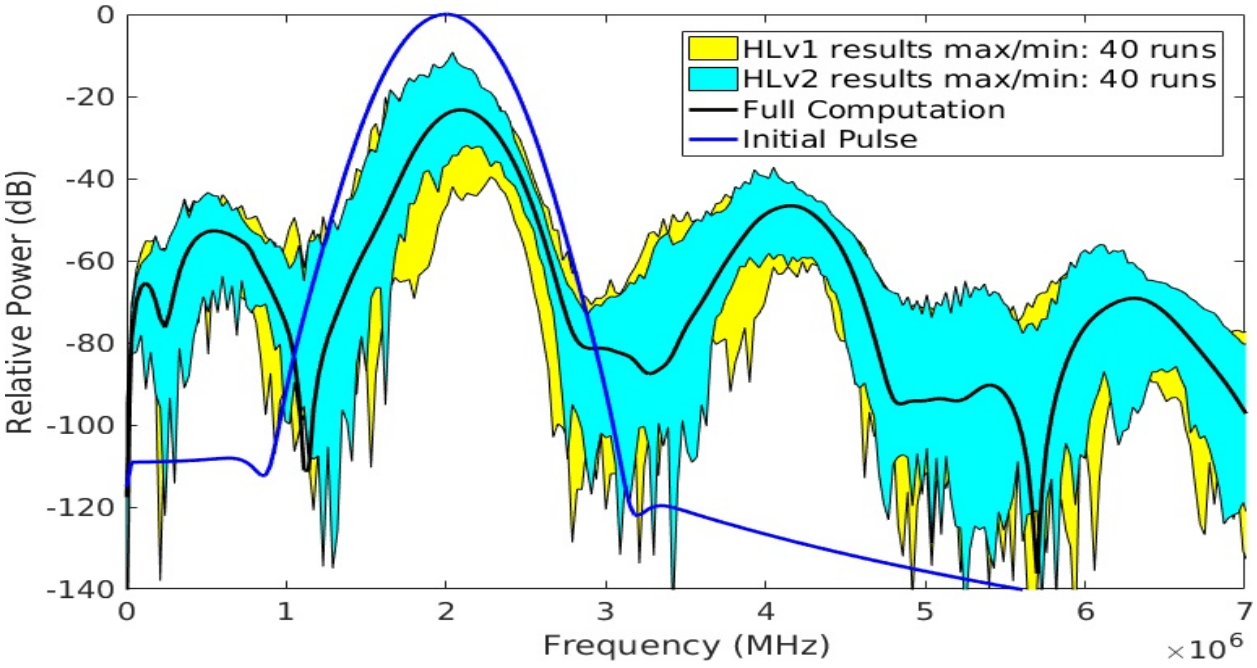

(a) HLv1 and HLv2 spread compared to fully polydisperse computation

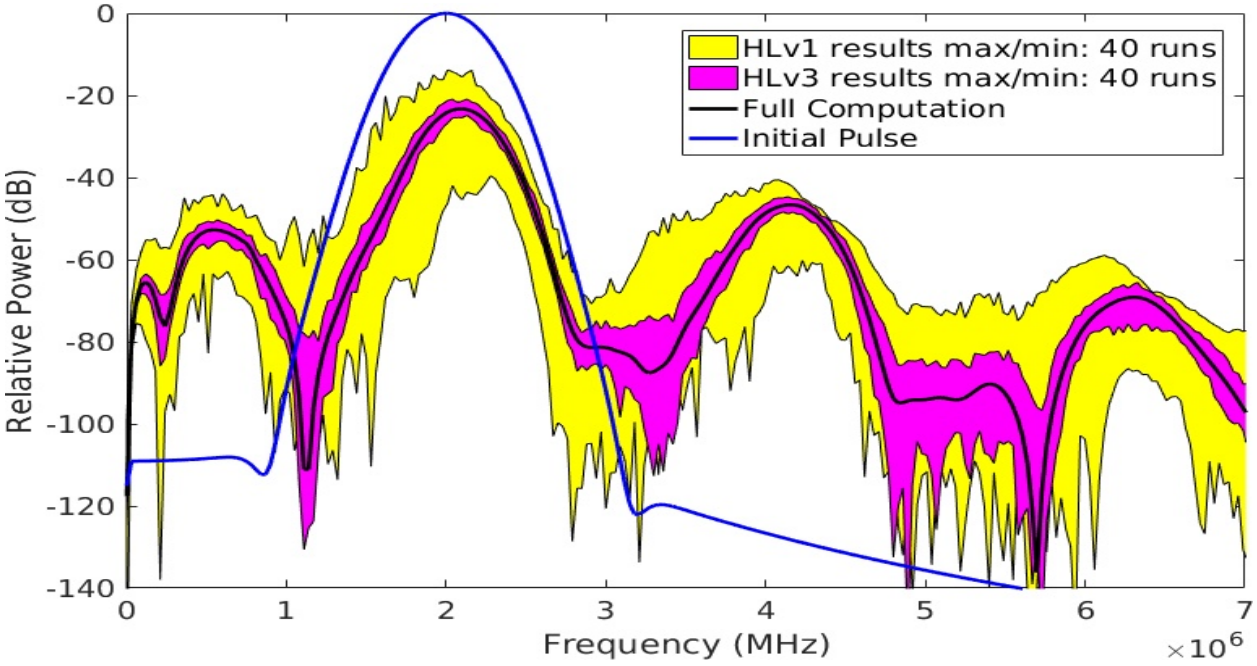

(b) HLv1 and HLv3 spread compared to fully polydisperse computation

Figure 9: Attenuation spectra for SonoVue® computations at incident frequency 2MHz with incident pulse amplitude 100kPa and SonoVue® concentration 10^{11} bubbles/m^3.

For a given incident frequency, incident pulse amplitude and concentration, an ensemble of 40 runs at 70 points per wavelength was computed for each HL strategy and a spectral analysis of the transmitted wave at 2cm was made for each run. The spectra obtained from the ensemble runs can then be compared to the spectrum from the transmitted wave obtained by the fully polydisperse computation. Figs. 9, 10 and 11 show the spread (i.e. the maximum and minimum extent) of the attenuated spectra obtained from the ensemble of 40 runs for each of the HL strategies, for three specific cases of different incident frequencies and pulse amplitudes. The fundamental, subharmonic and second harmonic responses are evident. It appears from all three figures that HLv1 has the largest variation in spectra obtained and, while HLv2 offers a marginal improvement in terms of less variation, the HLv3 ensemble runs have a significantly smaller variation in the spectra obtained. From all cases investigated, we conclude that a single run using HLv3 is expected to provide greater accuracy than the other two strategies. We also note that the averages of the spectra obtained for the fundamental, subharmonic and second harmonic responses for the HL computations always lie very close to the response obtained from the fully polydisperse calculation. An additional remarkable observation that can be made is that the ensemble spread is significantly greater for 2MHz than for the higher frequencies, and thus the accuracy of the HL approximation (for all strategies) seems to be greatly improved as the incident frequency increases.

These observations, for the most part, appear well explained by linear theory. The superiority of HLv3 in approximating the fully polydisperse calculation is due to the fact that maximising the λ/d ratio leads to a better approximation of the effective medium result obtained by the fully polydisperse computation. The significant reduction in spread as the incident frequency increases is rather surprising at first sight, as it cannot be explained by the intrinsic nonlinear resonant properties of SonoVue®. However, linear theory can explain this phenomenon by the fact that the relative difference in the impedance of neighbouring layers,

calculated in Sec. III.B using (6) and shown in Fig. 1, scales as the reciprocal of the cube of the frequency; thus the differences in layer impedance are significantly larger for 2 MHz than they are for the higher frequencies. Remarkably, linear theory appears able to predict quantitively how the spread of the nonlinear HLv3 ensembles varies with frequency to great accuracy. To demonstrate this, we first look at the attenuation of the fundamental peak and calculate an estimate of the standard deviation from the 40 values in the ensemble and then normalise this standard deviation using the magnitude of the mean attenuation from the fully polydisperse computation. We do this for the twenty nonlinear cases using HLv3 with different incident frequencies, amplitudes and SonoVue® concentrations and then plot the normalised standard deviations of the fundamental attenuation obtained from each ensemble on a graph. We also ran our linear code solving (12) for the Gorce et al.[5] distribution at $\lambda/d = 70$ with an ensemble of 5000 runs for each case. The result is Fig 12a, which shows that all the linear computations practically fall onto a single curve and the nonlinear results follow the same trend of a significantly narrower distribution of transmitted amplitudes at higher ultrasound frequencies. A similar calculation can then be performed for the relative attenuation of the second harmonic and subharmonic peaks and the plots of normalised standard deviations (normalised by the mean fundamental attenuation again) for the nonlinear cases are shown in Figs. 12b and 12c. While the trend is clearly weaker for the the second harmonic data it can clearly be observed again in the subharmonic peak. It can also be seen that the cases with the highest SonoVue® concentration lead to the largest normalised spread in the HLv3 predictions for the subharmonic and second harmonic responses; this is not the case, however, for the fundamental response.

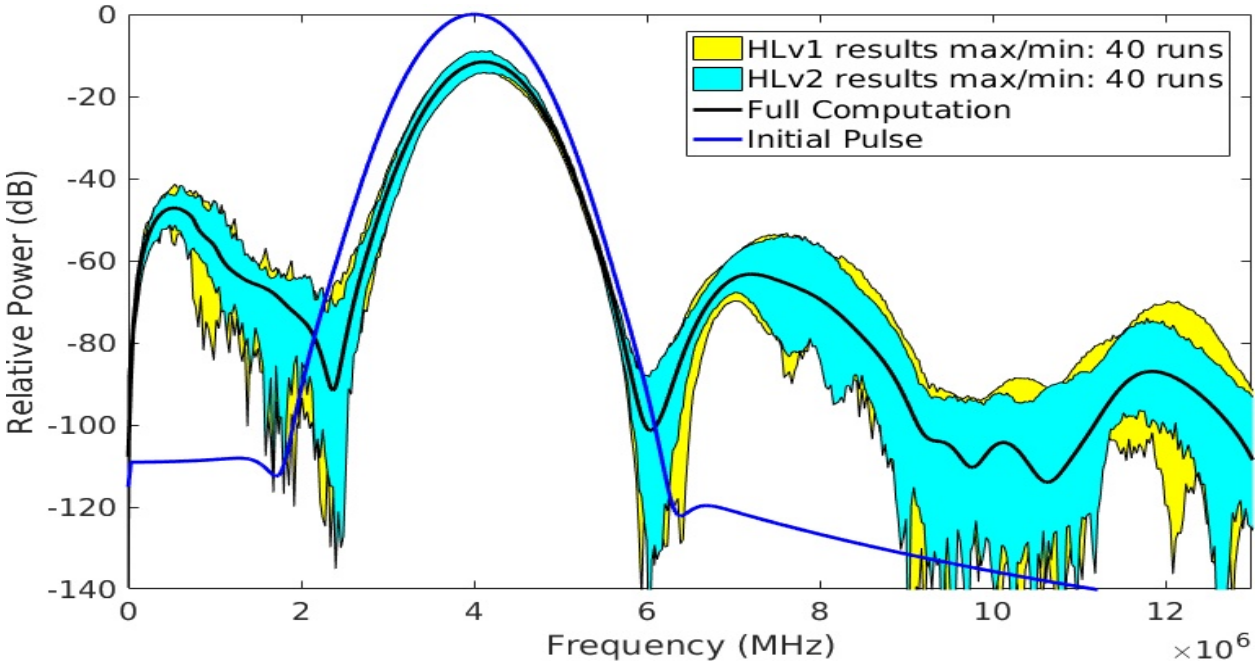

(a) HLv1 and HLv2 spread compared to fully polydisperse computation

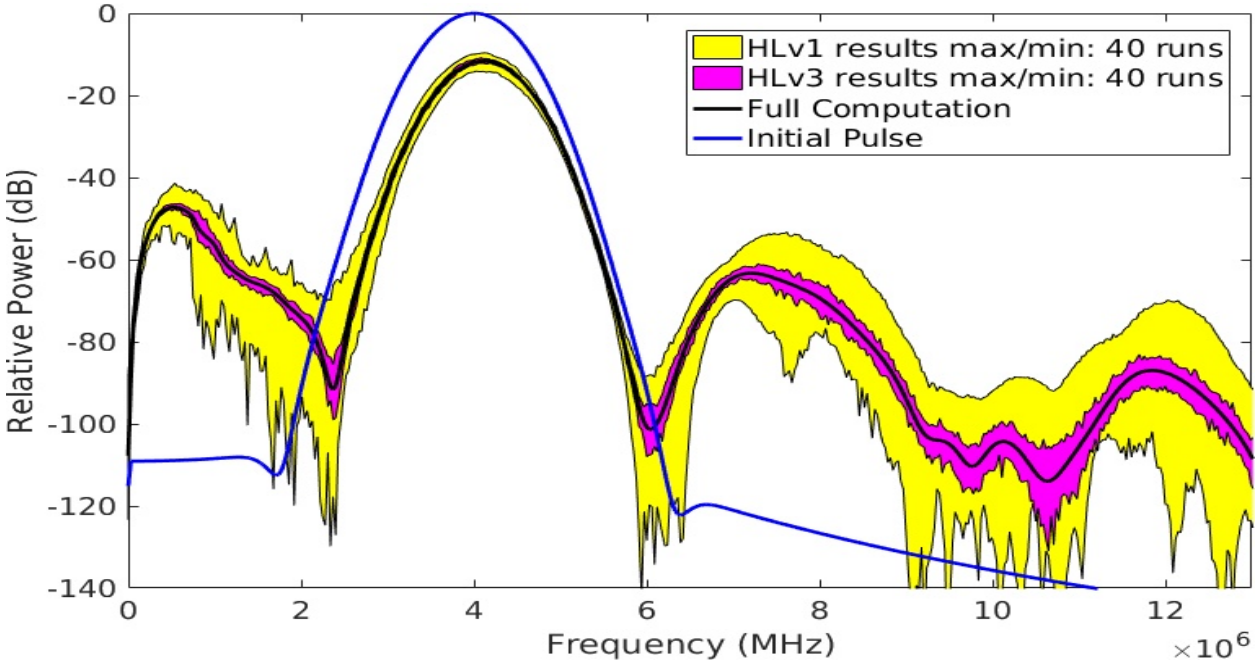

(b) HLv1 and HLv3 spread compared to fully polydisperse computation

Figure 10: Attenuation spectra for SonoVue® computations at incident frequency 4MHz with incident pulse amplitude 100kPa and SonoVue® concentration 10^{11} bubbles/m^3.

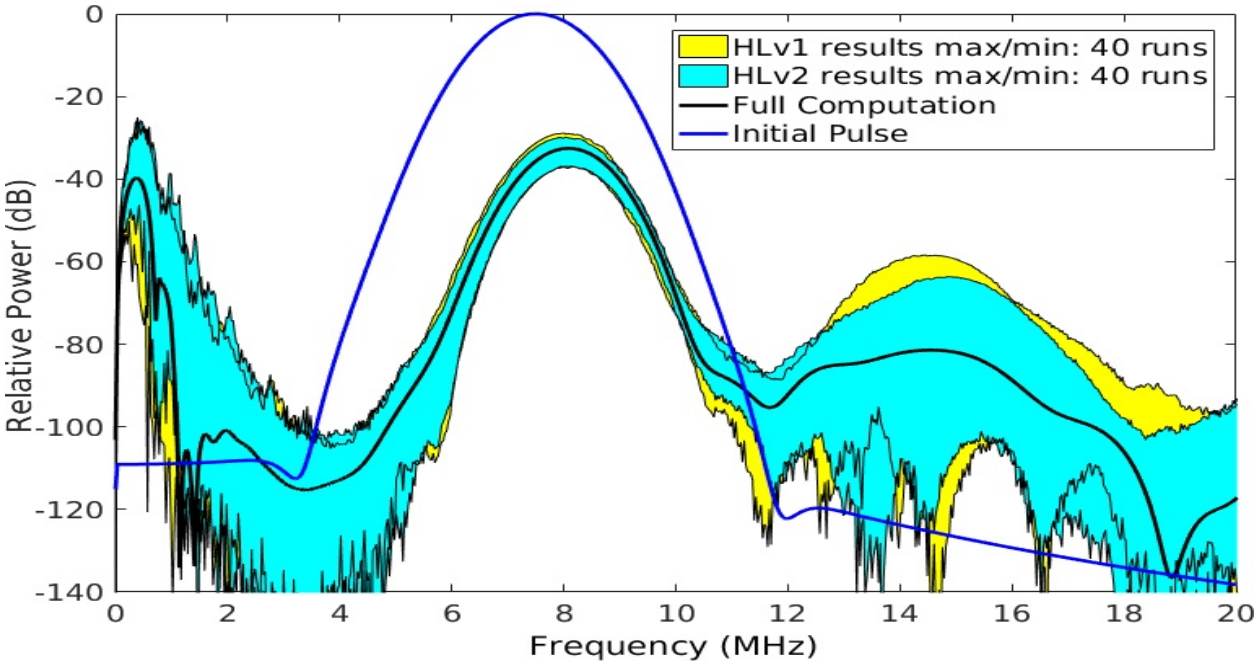

(a) HLv1 and HLv2 spread compared to fully polydisperse computation

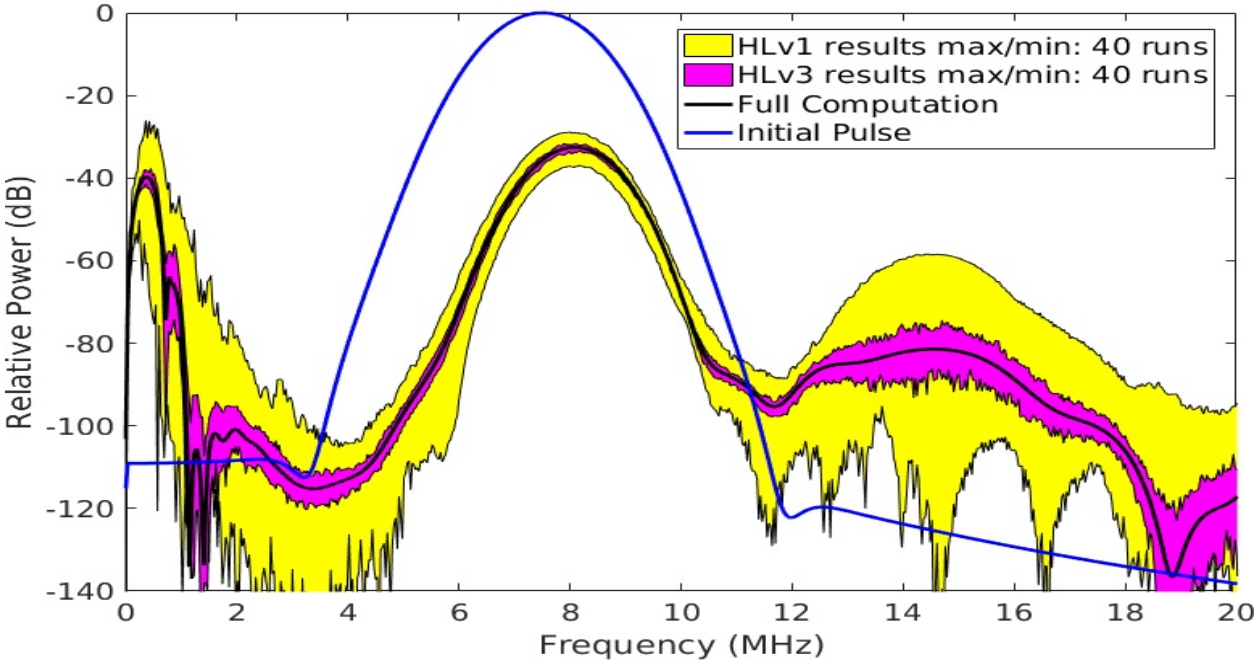

(b) HLv1 and HLv3 spread compared to fully polydisperse computation

Figure 11: Attenuation spectra for SonoVue® computations at incident frequency 7.5MHz with incident pulse amplitude 200kPa and SonoVue® concentration 10^{12} bubbles/m^3.

V Further analysis of the numerical results

A Validating the HL approximation

We now focus on the following important observations from the numerical results: (i) that the HL approximation appears optimal when λ/d is maximised and (ii) that the transmitted spectra obtained from running several HL computations at large λ/d form a distribution, the mean of which appears to be the result obtained from the fully polydisperse calculation. Further analysis is now presented here to theoretically confirm these observations and clarify the relationship between the fully polydisperse and HL computational approaches.

Consider the fully polydisperse nonlinear one-dimensional wave equation (1) which is nondimensionalised, as in the computations above, spatially on the characteristic (incident) wavelength, temporally by the characteristic (incident) frequency and with the pressure nondimensionalised by $\rho_0 c_0^2$. We assume here an incident ultrasound pulse travels through a polydisperse cloud with discrete *finite* bubble sizes N, where bubbles of nondimensional radius R_k, for $k = 1, \ldots, N$ occur at nondimensional concentrations n_k bubbles per unit volume. By careful integration along each set of characteristics[35] before converting back into space and time variables, the following implicit integral form of the equation can be obtained for the pressure at a certain point in space and time, *i.e.* $x = x_0$ and $t = t_0$:

$$p(x_0, t_0) = p_{\rm inc}(x_0 - t_0) + 2\pi \int_0^{t_0} \int_{x_0-(t_0-t')}^{x_0+(t_0-t')} \sum_{k=1}^{N} n_k G_k(x, t, p(x, t)) \mathrm{d}x' \mathrm{d}t'. \tag{15}$$

Here, $p_{\rm inc}(x-t)$ is the incident pressure pulse and $G_k(x, t, p) = R_k^2 \ddot{R}_k + 2R_k(\dot{R}_k)^2$ for bubbles of size R_k. For the HL approximation, its governing equation can be expressed in a similar way as follows:

$$p(x_0, t_0) = p_{\rm inc}(x_0 - t_0) + 2\pi \int_0^{t_0} n_{tot} \sum_{k=1}^{N} \left\{ \int_{\mathcal{E}_k(t')} G_k(x, t, p) \mathrm{d}x' \right\} \mathrm{d}t', \tag{16}$$

where $n_{tot} = \sum_{k=1}^{N} n_k$ and $\mathcal{E}_k(t')$ is the union of all layers of nondimensional thickness d containing bubble size k within the range $x_0 - (t_0 - t') \leqslant x \leqslant x_0 + (t_0 - t')$. The disjoint sets $\mathcal{E}_k(t')$ for $k = 1, \ldots, N$ therefore form a partition of the interval over which the integration of x takes place at time t', i.e. $\cup_{k=1}^{N} \mathcal{E}_k(t') = (x_0 - (t_0 - t'), x_0 + (t_0 - t'))$ and $\mathcal{E}_i(t') \cap \mathcal{E}_j(t') = \emptyset \, \forall i, j$ with $i \neq j$.

It is possible to interchange the bubble-size summation and integration in x in the fully polydisperse equation (15) and we propose that, as the layer thickness d tends to zero, equation (16) tends to the result of (15) if we can show at time t'

$$\lim_{d \to 0} \sum_{k=1}^{N} \left\{ n_{tot} \int_{\mathcal{E}_k(t')} G_k(x, t, p) \mathrm{d}x' \right\} = \sum_{k=1}^{N} \left\{ n_k \int_{x_0 - (t_0 - t')}^{x_0 + (t_0 - t')} G_k(x, t, p) \mathrm{d}x' \right\}. \tag{17}$$

To prove this, we initially assume that the interval width $2(t - t')$ has approximately $\mathcal{M}$ layers of thickness d. (with remainder less than d). We assume that $\mathcal{M}_k$ of those layers contain bubble size k. By selecting the bubble size k at random *without replacement* for each layer, we assert that $\mathcal{M}_k / \mathcal{M} = n_k / n_{tot} + \mathrm{O}(d/2(t - t'))$. Expressing $\mathcal{E}_k(t')$ as a union of intervals of thickness d, $\mathcal{E}_k(t') = \cup_{m=1}^{\mathcal{M}_k} (x_{km} - d/2, x_{km} + d/2)$, and then expanding the integrand using a Taylor series yields

$$n_{tot} \int_{\mathcal{E}_k(t')} G_k(x, t, p) \mathrm{d}x' = n_{tot} d \sum_{m=1}^{\mathcal{M}_k} G_k(x_{km}, t', p(x_{km}, t')) + \mathrm{O}(d^2). \tag{18}$$

Given that $n_{tot}/n_k = 2(t_0 - t')/\mathcal{M}_k d + \mathrm{O}(d)$ we then find that

$$n_{tot} \int_{\mathcal{E}_k(t')} G_k(x, t, p) \mathrm{d}x' = n_k \frac{2(t_0 - t')}{\mathcal{M}_k} \sum_{m=1}^{\mathcal{M}_\parallel} G_k(x_{km}, t', p(x_{km}, t')) + \mathrm{O}(d^2). \tag{19}$$

This expression clearly demonstrates that the HL approximation is an example of Monte Carlo integration[36], where a random sampling of $\mathcal{M}_k$ values within the domain of interest is used to determine the integral contribution from each bubble size k. By the law of large

numbers and the mean value theorem, we can be certain that as $d \to 0$, and consequently $\mathcal{M}_k \to \infty$, the sample mean tends to its expected value. Thus

$$n_k \frac{2(t_0 - t')}{\mathcal{M}_k} \sum_{m=1}^{\mathcal{M}_\parallel} G_k(x_{km}, t', p(x_{km}, t')) \to n_k \int_{x_0-(t_0-t')}^{x_0+(t_0-t')} G_k(x, t, p) \mathrm{d}x', \tag{20}$$

for each bubble size k and the proposed limit (17) over the sum of all bubble sizes is proven. The transmitted wave from the fully polydisperse nonlinear wave equation and the transmitted wave obtained from the HL approximation will therefore coincide as the layer thickness tends to zero. Note that any other limit (e.g. $t_0 \to \infty$) does not lead to such convergence. However, as long as λ/d is large and well away from the transition region, any results obtained from the HL approach come from a distribution, the expected value of which is the result obtained from the full approximation; this theoretically confirms points (i) and (ii) observed in the numerical results above.

B Computational efficiency of the HL approximation

Given that HL calculations lead to a distribution of values, one final question tackled here is whether a trade off in accuracy exists between a single HL calculation performed on a very fine grid and an average of several HL calculations performed on a coarser grid. Table II shows unbiased standard deviations calculated from 40 HLv3 runs for several different nonlinear cases on computational grids with points per wavelength (ppw) of 20, 35 and 70. As the computational effort (*i.e.* time) of such a run is roughly proportional to the points per wavelength squared, it is possible to run $(70/20)^2 \approx 12$ runs at 20ppw and $(70/35)^2 = 4$ runs at 35ppw for the same effort as a single 70ppw run. By assuming that the central limit theorem holds it the makes sense to compare the standard deviation σ_{70} of the attenuation calculated from a single 70ppw run to the standard deviation from the mean of 4 runs at 35ppw, *i.e.* $\sigma_{35}/\sqrt{4}$, and the mean of 12 runs at 20 ppw, *i.e.* $\sigma_{20}/\sqrt{12}$. The cell containing

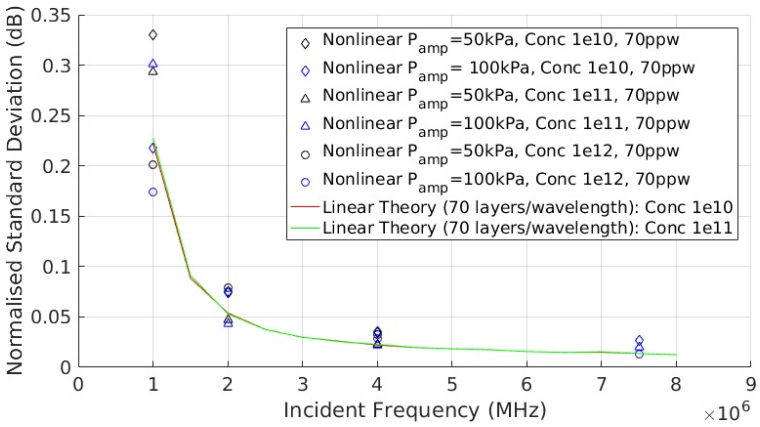

(a) Normalised standard deviation for fundamental response.

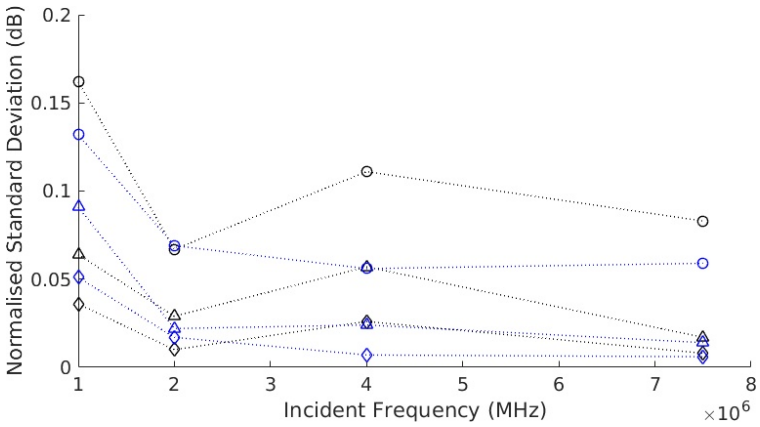

(b) Normalised standard deviation for second harmonic response.

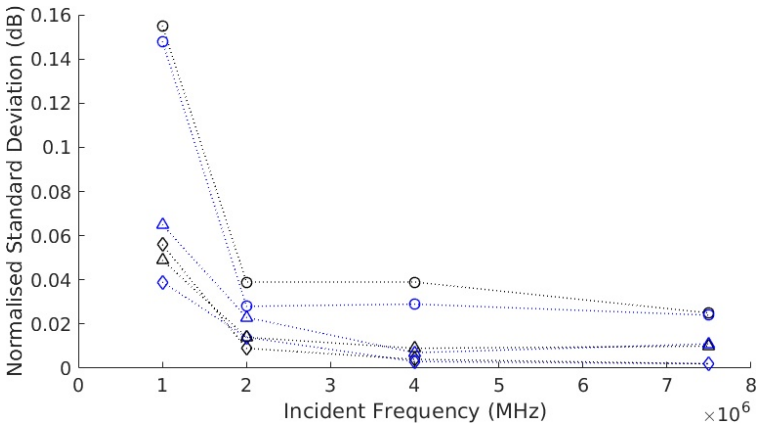

(c) Normalised standard deviation for subharmonic response.

Figure 12: Normalised standard deviations obtained from nonlinear HLv3 computations versus those obtained from linear HL theory.

the smallest of these values for each case is labelled with an asterisk.

Firstly we can see from Table II that a single HLv3 run is more likely to accurately replicate the response of the fully polydisperse nonlinear computation as the points per wavelength increases. While some of this improving accuracy can be attributed to the finer finite-difference grid used, a significant component is actually achieved due to the higher λ/d ratio leading to more accurate approximation of the effective medium. Higher ppws require significantly more computational effort and, for the case of accurately predicting the fundamental attenuation and subharmonic response, it would seem that the additional accuracy gained from increasing the ppw, to consequently raise the λ/d ratio, cannot always be justified when compared to running several parallel HLv3 runs using a coarser grid and taking an average of their results. This conclusion is backed up by the fact that the differences in the mean attenuation obtained from the HLv3 ensembles from 20ppw, 35ppw and 70ppw calculations are small in magnitude compared to the overall spread of the ensemble results. Unfortunately, such a coarser averaging approach does not appear optimal when trying to accurately replicate the second harmonic response, which suggests fewer HLv3 runs averaged over a finer grid may achieve a more accurate result. Such an observation, however, makes intuitive sense as the second harmonic is a wave of higher frequency and therefore accurate resolution of these higher harmonics necessitates a finer grid than that required for the fundamental and subharmonic components.

VI Conclusions

Accurate quantification of tissue perfusion and other physiologically relevant measures requires accurate interpretation of the backscattered signal from microbubble populations. Despite the advent of supercomputing resources and the parallelisation of propagation codes,

Table II: Estimates of standard deviation taken from 40 HLv3 runs on finite-difference grids with 20ppw, 35ppw and 70ppw. The starred value suggests the most accurate when averages are taken of several runs based on equal computational effort.

	Fundamental				Second Harm				Subharmonic			
Freq P_{amp} Conc	Full dB	σ_{20}	σ_{35}	σ_{70}	Full dB	σ_{20}	σ_{35}	σ_{70}	Full dB	σ_{20}	σ_{35}	σ_{70}
4MHz 50kPa 1e10	-1.2	*0.06	0.05	0.04	-107.8	*7.55	4.47	2.78	-78.6	0.57	*0.30	0.30
4MHz 100kPa 1e10	-1.1	*0.06	0.05	0.04	-96.4	4.65	*1.10	0.71	-82.5	*0.52	0.35	0.23
4MHz 200kPa 1e10	-1.1	*0.05	0.04	0.04	-91.6	2.69	*0.77	0.49	-82.2	*0.75	0.50	0.30
4MHz 50kPa 1e11	-12.2	*0.56	0.39	0.28	-81.1	12.71	*5.46	4.62	-44.5	*0.65	0.66	0.40
4MHz 100kPa 1e11	-12.0	*0.55	0.38	0.27	-69.5	11.08	*3.15	1.65	-47.2	*0.77	0.61	0.33
4MHz 200kPa 1e11	-11.1	*0.50	0.35	0.25	-60.8	7.09	*0.84	0.65	-57.7	*0.84	0.57	0.45
4MHz 50kPa 1e12	-124.4	*4.94	3.22	4.04	-103.9	*13.71	9.21	11.55	-39.6	*2.75	2.01	1.53
4MHz 100kPa 1e12	-128.3	*5.46	3.60	3.75	-98.0	13.18	*7.01	5.54	-37.2	*2.05	1.94	1.09
4MHz 200kPa 1e12	-130.8	7.05	*3.80	2.43	-90.9	6.15	*3.52	2.84	-39.1	*2.31	1.46	1.21
7.5MHz 50kPa 1e10	-0.3	*0.02	0.01	0.01	-123.3	*2.83	2.58	0.99	-91.1	*0.39	0.29	0.19
7.5MHz 100kPa 1e10	-0.3	*0.02	0.01	0.01	-117.0	2.51	1.95	*0.67	-88.8	*0.35	0.23	0.20
7.5MHz 200kPa 1e10	-0.3	*0.02	0.01	0.01	-110.1	1.60	0.98	*0.35	-87.8	*0.30	0.19	0.13
7.5MHz 50kPa 1e11	-3.3	*0.14	0.09	0.07	-97.5	10.53	7.54	*1.70	-62.1	*1.00	0.88	0.62
7.5MHz 100kPa 1e11	-3.3	*0.14	0.09	0.07	-89.3	10.77	5.26	*1.22	-57.5	*1.25	1.04	0.63
7.5MHz 200kPa 1e11	-3.3	*0.14	0.09	0.07	-79.9	5.30	2.02	*0.60	-55.4	*1.13	0.87	0.58
7.5MHz 50kPa 1e12	-34.5	*0.69	0.59	0.43	-99.2	*8.41	10.36	8.26	-54.2	*2.79	1.70	1.37
7.5MHz 100kPa 1e12	-34.6	*0.73	0.59	0.44	-90.3	*10.74	7.86	5.32	-46.3	*2.26	1.67	1.09
7.5MHz 200kPa 1e12	-35.7	*0.84	0.64	0.48	-82.0	11.86	*5.65	3.03	-39.7	*2.03	1.30	0.85

the simulation of ultrasound propagation through microbubble populations still represents a formidable numerical task. Consequently, efficient computational algorithms that have the potential to be implemented in real-time on clinical scanners, such as the HL approach proposed by Hibbs et al[22], remain highly desirable.

The results obtained from linear theory on how the consequent layering of bubbly media, via implementing the HL approach, affects wave transmission provides useful insight into the effect of wavelength-to-layer-width ratio and the possible occurrence of shielding phenomena. Numerical simulations of bidisperse bubble populations subsequently confirm that such phenomena still arise when applying the HL approach to clinically relevant fully nonlinear cases that involve higher amplitudes and resonant bubbles. Importantly, linear theory points to crucial modifications to the original HL strategy proposed by Hibbs et al.[22] that improve its accuracy in approximating the fully polydisperse *effective medium* computation, wherein the response of all bubbles sizes is included at every grid point. The suggested modifications are: (i) use large λ/d ratios greater than 10 and, therefore, do not use mean bubble separation distance; and (ii) use random choice without replacement in order that the number of layers of each bubble size equals the expected value.

From our numerical simulations on propagation through polydisperse bubble populations, involving clinically relevant ultrasound frequencies, pressure amplitudes and clinically relevant concentrations of SonoVue®, the strategy HLv3 proposed in this paper is shown to provide a much closer approximation to the fully polydisperse computation than the original HLv1 approach of Hibbs et al[22]. The typical estimated standard deviation (dB scale) from HLv3 was one quarter to one sixth of the standard deviation obtained from the HLv1 strategy across all frequencies and we note that HLv3 has *no* additional computation overheads compared to the original HLv1 strategy. The ensembles of 40 computations for each of the HL strategies result in a distribution of spectra, the mean of which in all cases is the

spectra obtained from the fully polydisperse calculation. These observations are backed up by further analysis that demonstrates the HL approach is a form of Monte-Carlo integration method of solving the fully polydisperse calculation and the solution obtained by the HL approach will converge to the fully polydisperse computation in the limit of zero layer thickness.

Although Hibbs et al.'s numerical simulations using HLv1[22] demonstrate increased nonlinear behaviour in the results obtained, akin to that observed in experiments but not apparently captured by the fully polydisperse nonlinear wave equation (2), their conclusion is not confirmed by the distribution of HL runs in Figs. 9 to 11 and the subsequent analysis in Sec. V.A. Our work strongly suggests that HL computations are equally likely to show higher or lower nonlinearity than the fully polydisperse model. Hence, their results cannot be viewed as a prediction of realistic phenomena of a disperse bubble cloud in a clinical setting and it can only be assumed that the increased nonlinear behaviour is an artefact of the coarse grid and unphysical layering used. Therefore, some questions remain unanswered regarding how to better predict the nonlinear response of ultrasound propagation through bubble clouds.

The observation made, via our nonlinear computations and strongly supported by linear theory, that an HL approximation of a commercial polydisperse bubble cloud improves at higher frequencies is a very significant and important result because the high frequency regime is where reducing the computational effort becomes a real and vital challenge. Thus, the HLv3 strategy offers an efficient computational scheme that could prove crucial to achieving real-time computational at clinically-relevant ultrasound frequencies. Our numerical simulations of HLv3 computations over finite-difference grids with different points per wavelength indicate that taking an average of several parallel HLv3 runs on a coarser grid is a more computationally efficient way to resolve the fundamental attenuation and subharmonic

response than taking significantly fewer runs on a fine grid. This, again, is backed up by the analysis in Sec. V.A confirming that the HL is a sampling Monte-Carlo approach to integrate the wave equation. Resolving the higher harmonics, however, still requires a suitably finer grid which evidently leads to some trade off between the points per wavelength and the number of HLv3 runs used to determine an average response.

Future work will aim to demonstrate the viability of the HLv3 approach by comparing its predictions to experimental data on ultrasound propagation through polydisperse microbubble suspensions. Simulations and experiments on polydisperse bubble populations other than SonoVue® are required, in addition to incorporating variations in coating parameters between different bubbles, which contributes to the spread of resonance frequencies in practice, as well as surfactant shedding. Moreover, to accurately simulate microbubble contrast agents in clinical settings, issues such as realistically simulating the response of bubbles located in blood vessels or tissue must be addressed, incorporating the obvious fact that the underlying medium is not a homogeneous Newtonian liquid. More concentrated suspensions will also result in highly complex interactions between neighbouring bubbles that are likely to significantly alter the scattered field.

Acknowledgements

This work was supported by the Engineering and Physical Sciences Research Council via grant EP/I021795/1 and via J-P. O'Brien's doctoral training grant. We are extremely grateful to Meng-Xing Tang and Robert Eckersley for their thoughtful comments and helpful suggestions regarding this research.

REFERENCES

[1] J. R. Lindner, "Microbubbles in medical imaging: current applications and future directions", Nature Reviews Drug Discovery **3**, 527–533 (2004).

[2] D. Cosgrove and N. Lassau, "Imaging of perfusion using ultrasound", Eur. J. Nucl. Med. Mol. Imaging **37**, S65–S85 (2010).

[3] M. Tang, H. Mulvana, T. Gauthier, A. Lim, D. Cosgrove, R. Eckersley, and E. Stride, "Quantitative contrast-enhanced ultrasound imaging: a review of sources of variability", Interface Focus **1**, 520–539 (2011).

[4] G. Renaud, J. Bosch, G. Ten Kate, V. Shamdasani, R. Entrekin, N. de Jong, and A. Van der Steen, "Counter-propagating wave interaction for contrast-enhanced ultrasound imaging", Physics in medicine and biology **57**, L9 (2012).

[5] J.-M. Gorce, M. Arditi, and M. Schneider, "Influence of bubble size distribution on the echogenicity of ultrasound contrast agents: A study of sonovue$^{\mathrm{TM}}$", Investigative radiology **35**, 661–671 (2000).

[6] K. P. Davy and D. R. Seals, "Total blood volume in healthy young and older men", Journal of Applied Physiology **76**, 2059–2062 (1994).

[7] J. W. Strutt, "LVIII. on the scattering of light by small particles", The London, Edinburgh, and Dublin Philosophical Magazine and Journal of Science **41**, 447–454 (1871).

[8] J. W. S. B. Rayleigh, *The theory of sound*, volume 2 (Macmillan) (1896).

[9] C. Sewell, "The extinction of sound in a viscous atmosphere by small obstacles of cylindrical and spherical form", Philosophical Transactions of the Royal Society of London. Series A, Containing Papers of a Mathematical or Physical Character **210**, 239–270 (1911).

[10] E. Carstensen and L. Foldy, "Propagation of sound through a liquid containing bubbles", The Journal of the Acoustical Society of America **19**, 481–501 (1947).

[11] S. Iordanskii, "On the equations of liquid motion with gas bubbles", Zh. Prikl. Mekh. i Tekh. Fiz **1**, 102–110 (1960).

[12] V. Kedrinskii, "Propagation of perturbations in a liquid containing gas bubbles", Journal of Applied Mechanics and Technical Physics **9**, 370–376 (1968).

[13] N. Gumerov, "Quasi-monochromatic weakly non-linear waves in a low-dispersion bubble medium", Journal of Applied Mathematics and Mechanics **56**, 50–59 (1992).

[14] N. Gumerov, "Propagation of long waves of finite amplitude in a liquid with polydispersed gas bubbles", Journal of applied mechanics and technical physics **33**, 79–85 (1992).

[15] K. Ando, T. Colonius, and C. E. Brennen, "Numerical simulation of shock propagation in a polydisperse bubbly liquid", International Journal of Multiphase Flow **37**, 596–608 (2011).

[16] L. van Wijngaarden, "On the equations of motion for mixtures of liquid and gas bubbles", Journal of Fluid Mechanics **33**, 465–474 (1968).

[17] R. Caflisch, M. Miksis, G. Papanicolaou, and L. Ting, "Effective equations for wave propagation in bubbly liquids", J. Fluid Mech. **153**, 259–273 (1985).

[18] K. Commander and A. Prosperetti, "Linear pressure waves in bubbly liquids: comparison between theory and experiments", J. Acoust. Soc. Am. **85**, 732–746 (1989).

[19] E. Stride and N. Saffari, "Investigating the significance of multiple scattering in ultrasound contrast agent particle populations", IEEE Trans on Ultrasonics, Ferroelectrics and Freq Control **52**, 2332–2345 (2005).

[20] M.-X. Tang and R. Eckersley, "Nonlinear propagation of ultrasound through microbubble contrast agents and implications for imaging", IEEE Transactions on Ultrasonics, Ferroelectrics and Frequency Control **53**, 2406–2415 (2006).

[21] J.-P. O'Brien, E. Stride, and N. Ovenden, "Surfactant shedding and gas diffusion during pulsed ultrasound through a microbubble contrast agent suspension", The Journal of the Acoustical Society of America **134**, 1416–1427 (2013).

[22] K. Hibbs, J.-M. Mari, E. Stride, R. Eckersley, A. Noble, and M.-X. Tang, "P4d-7 nonlinear propagation of ultrasound through microbubble clouds: A novel numerical implementation.", Ultrasound Symposium. IEEE **2007**, 1997–2000 (2007).

[23] W. Lauterborn, "Numerical investigation of nonlinear oscillations of gas bubbles in liquids", The Journal of the Acoustical Society of America **59**, 283–293 (1976).

[24] E. Stride, "The influence of surface adsorption on microbubble dynamics", Phil. Trans. R. Soc. A **366**, 2103–2115 (2008).

[25] P. Marmottant, S. van der Meer, M. E. M. Versluis, N. de Jong, S. Hilgenfeldt, and D. Lohse, "A model for large amplitude oscillations of coated bubbles accounting for buckling and rupture", J. Acoust. Soc. Am. **118**, 3499–3505 (2005).

[26] D. Chatterjee and K. Sarkar, "A newtonian rheological model for the interface of microbubble contrast agents", Ultrasound med. biol. **29**, 1749–1757 (2003).

[27] D. J. Griffiths and C. A. Steinke, "Waves in locally periodic media", American Journal of Physics **69**, 137–154 (2001), URL `http://dx.doi.org/10.1119/1.1308266`.

[28] A. Stovas and Y. Roganov, "Acoustic waves in layered media - from theory to seismic applications", in *Waves in Fluids and Solids*, edited by R. P. Vila (InTech, Rijeka, Croatia) (2011), URL `http://www.intechopen.com/books/waves-in-fluids-and-solids/acoustic-waves-in-layered-media-from-theory-to-seismic-applications`.

[29] D. Sprung, H. Wu, and J. Martorell, "Scattering by a finite periodic potential", American Journal of Physics **61**, 1118–1124 (1993).

[30] J. M. Hovem, "Acoustic waves in finely layered media", Geophysics **60**, 1217–1221 (1995).

[31] A. Stovas and B. Arntsen, "Vertical propagation of low-frequency waves in finely layered media", Geophysics **71**, T87–T94 (2006).

[32] J. Carcione, D. Kosloff, and A. Behle, "Long-wave anisotropy in stratified media: A numerical test", Geophysics **56**, 245–254 (1991).

[33] Z. Ye and H. Hsu, "Phase transition and acoustic localization in arrays of air bubbles in water", Applied Physics Letters **79**, 1724–1726 (2001).

[34] J.-P. O'Brien, N. Ovenden, and E. Stride, "Accounting for the stability of microbubbles to multi-pulse excitation using a lipid-shedding model", The Journal of the Acoustical Society of America **130**, EL180–EL185 (2011).

[35] H. F. Weinberger, *A first course in partial differential equations: with complex variables and transform methods* (Dover Publications) (1995).

[36] G. P. Lepage, "A new algorithm for adaptive multidimensional integration", Journal of Computational Physics **27**, 192–203 (1978).